Research Article

Reduction of the Influence of Interfering Signals on the Longitudinal Control of UAVs with Fixed Wing

Róbert Bréda ⬤ **, Šimon Karaffa** ⬤ **, Rudolf Andoga** ⬤ **, and Miriam Hlinková** ⬤

Department of Avionics, Faculty of Aeronautics, Technical University of Košice, 040 01 Košice, Slovakia

Correspondence should be addressed to Šimon Karaffa; simon.karaffa@tuke.sk

The presented study offers a comprehensive insight in design and application of the Kalman filters for improvement of control efficiency of small unmanned aerial vehicles with fixed wing. The presented control scheme of the UAV includes its model, a servo drive model, and an optimal proportional-integral-derivative (PID) controller for the selected flight speed. Subsequently, process noise and measurement noise components were introduced into the whole constructed UAV model. The process noise was formed by disturbances caused by horizontal and vertical airflow in the atmosphere. The measurement noise contained deterministic and stochastic errors of the inertial measurement unit (IMU) UAV sensors and engine noise. The obtained results showed that the designed optimal Kalman filter was able to eliminate the influence of interfering signals from the control process and increased the phase safety, controllability, and stability of UAV control as a lean design can be applied in real-time control systems like Pixhawk PX4.

1. Introduction

A large group of sensors installed in the UAV inertial measurement units is based on micro-electromechanical system (MEMS). These sensors have limited accuracy, so it is necessary to correct the sensor noise that affects measurement accuracy. The impact of positional and sensor errors requires the solution of a complex mathematical apparatus [1, 2]. The individual components of the three-axis gyroscopes and accelerometers affect the accuracy of the individual channels of the UAV control and navigation system [3]. Errors occur between individual channels due to the transformation of acceleration. The accuracy of the primary sources of the UAV's inertial measurement unit is determined by environmental temperature changes and vibrations.

Interfering signals may affect the overall stability of UAV control. Interference consists of the noise mechanisms of the IMU UAV's inertial measuring unit sensors, the surrounding atmosphere, the operation of the engine, and the pilot inputs to the control. The UAV contains a control unit Pixhawk, which is part of the avionic equipment used by the UAV "Skydog." The unit provides data collection from

the IMU sensors and performs calculations and processing of these data. The UAV control system operates in a closed loop that contains an IMU with sensors to determine the position of the UAV.

Disturbance signals can affect the overall stability of UAV control. Interference can be caused by noise from the sensors of the UAV's inertial measurement unit (IMU), the surrounding atmosphere, the engine operation, and the pilot inputs into the control. The UAV used in the study contains the Pixhawk control unit, which is part of its avionic equipment. The unit ensures data collection from IMU sensors and performs calculations and processing of this data. The UAV control system operates in a closed loop, which includes IMU with sensors to determine the position of the UAV.

The internal control loop of the UAV performs its primary stabilization, while the outer loop performs tasks related to the UAV's manoeuvring and navigation. The analysis performed, with an emphasis on the accuracy of the UAV's IMU sensors, plays a decisive role in autonomous navigation using integration algorithms [4]. The Kalman filter in the UAV control circuit is used to estimate the state variables of the UAV system for given measurements of

output signals of the system, including measurement and process noise. Static measurements of the Pixhawk PX4 IMU sensors are required to determine the measurement noise parameters. The analysis is performed for all three axes of the Pixhawk PX4 IMU accelerometers and gyroscopes using standardized procedures [5, 6]. For longitudinal UAV movement, it is primarily necessary to analyse the gyroscope data on the Y-axis.

The design of new UAV control algorithms can be implemented in the Matlab/Simulink simulation environment using the PX4 Autopilot Support from Embedded Coder software. The software can generate C++ (object-oriented computer language) code from the Simulink simulation environment. The code structure is compatible with the Pixhawk PX4 autopilot software. The proposed algorithms can be changed and adapted as needed or completely replace the Pixhawk PX4 control system. For control commands from the remote control (RC) transmitter, it is possible to use input blocks, which can be used to adjust the control signal. The modified signal can be used as input for the "pulse-width modulation (PWM) output" block, which represents the control servos attached to the control surfaces of the UAV. With the use of libraries in the Matlab/Simulink program, it is possible to use individual blocks of sensors that will generate data from the analysed sensors of accelerometers and gyroscopes. To implement the proposed algorithms in the Pixhawk PX4 autopilot unit, it is necessary to install the necessary "Cygwin toolchain" interface [7].

The design of a suitable control system for a small fixed wing UAV must be preceded by the creation of a mathematical simulation model to assess the optimal UAV control algorithm's influence on its properties under the influence of disturbing signals. The mathematical simulation model is based on physical quantities obtained during experimental flights and measurements of its aerodynamic and mechanical properties. This model is used to design an optimal controller, which is analysed by changing its coefficients as the UAV's flight speed changes. The optimal controller can be verified by the real flight of the UAV and a mathematical model with six degrees of freedom (6DoF). Using the 6DoF model of a small fixed wing UAV, inputs represent elevator deflection, and outputs that are represented by the angular velocity of pitch angle ϑ are obtained. The proposed control system for UAVs with an optimal controller is extended by a Kalman filter.

The Allan variation method can be used to analyse the sensors of the Pixhawk PX4 autopilot. The method is a possible equivalent of the power spectrum in time. Allan's variance is a tool that graphically displays the performance of the analysed signal. It displays the signal as a function of time the averaged sensor output subparts compared to a graphical representation of the signal power as a function of frequency. The use of Allan's variance is determined by the Institute of Electrical and Electronic Engineers (IEEE) standard, which defines not only its application but also the procedure by which the results are analysed. The result is a representation of noises in the output of the IMU sensors in terms of long-term time development. The slopes of the straight lines represent the individual types of noise represented in the output of the Pixhawk PX4 IMU sensors [6].

Atmospheric turbulence is one of the sources of UAV control errors. Turbulence is the movement of air caused by the unstable distribution of pressure and temperature in clouds near the earth and in the area of currents. Atmospheric turbulence can be defined as a stochastic process determined by velocity. Of the disturbances that affect the UAV during flight and landing, the moments are caused by horizontal and vertical airflow. Turbulent flow is characterized by the fact that the velocity at a given point varies considerably and irregularly. A sudden gust of wind acting on the UAV from below results in an increase in the angle of attack. The random component of the wind speed vector represented by the turbulence of the atmosphere affects the short-term oscillations and position angles of the UAV [8]. The pilot is one of the members of the UAV control loop, and their good training can reduce the control deviation. Other interfering signals are introduced into the UAV control process by the operation of the engine.

The control loop of the UAV includes feedback from sensors that contain various types of noise and interference in addition to the required information. These noises and disturbances are processed by control systems and therefore need to be identified [9]. The sensor error model and Alan's variation can be used to identify sensor errors. When creating a sensor error model, it is necessary to perform a long-term static measurement from which sensor errors are identified [4]. Based on the knowledge of the sensor error model, it is possible to design an optimal linear-quadratic-Gaussian (LQG) controller for the UAV control system [10]. In the kinematic vehicle, models are used together with IMU, global navigation satellite system (GNSS), and multidirectional airspeed sensors to estimate the wind field [11]. The work focused on approaches using aircraft models that fully model the aerodynamic and kinematic behaviour of UAVs [12]. Ravi Kumar and Dr Ramamurthy, in their paper in 2015 [13], validated a model of aircraft inclination, tilt, and side slip control using an linear-quadratic regulator (LQR) controller and an LQG controller. The results of the simulation and analysis showed that the linear-quadratic regulator (LQR) controller delivered relatively better performance. The LQG controller achieved very good results with an output device with limited constant shift error, and the Kalman filter was the optimal estimator when working with Gaussian white noise. LQR control is used with a Kalman filter (KF) that estimates the real states of the system in noisy environments in state feedback servo control systems [14]. Based on [15, 16], it can be stated that PID, LQR, and LQG controllers can be used to increase the stabilization of the pitch angle. The use of one regulator will increase the stability of the UAV and reduce the impact of noise that may occur in the control process. The system's response to the required change is shortened, and unwanted oscillations are also eliminated. According to [17], random vibrations caused by the UAV engine or external influences must also be considered in the process of estimating the optimal state of the system. Li et al. [18] improved the longitudinal static stability and dynamic properties of the UAV flying wing by designing an extended robust LQR.

Thanks to non-Gaussian methods, new concepts of approximation methodologies for optimal filtration that are more efficient than the Kalman one have been developed

[19]. The most popular methods in this area are the unscented and extended Kalman filters [20] as well as methods based on particle filtering. These methods are however quite complex to develop and implement in real-time systems with limited computational power [21].

Based on the previous study, the aim of the present research was to design an optimal standard Kalman filter, which should be able to reduce interfering signals acting on Pixhawk PX4 sensors by extending the control scheme applied on a fixed wing unmanned aerial vehicle. The optimally designed standard Kalman filter is aimed at applying real-time control systems improving its phase safety, manoeuvrability, and control stability in general by application of precise analysis of disturbing signals acting on the UAV.

2. Materials and Methods

The object of observation was an unmanned aerial vehicle with a fixed wing, called "Skydog" (UAV). Due to its flight control and mechanical similarity with general aircraft, it can be used to perform experiments in the field of autonomous aircraft control. The wingspan of the UAV "Skydog" is 2.3 meters, the basic empty weight is 6.85 kilograms, and the maximum take-off weight is 8.65 kilograms. The UAV is able to carry the necessary measuring equipment or small experimental equipment.

2.1. Dynamic Modelling of UAV Flight. During the flight, several different types of forces act on the UAV, the interaction of which affects the movement and position of the UAV in space. According to the basic understanding, there are four forces: lift, thrust, aerodynamic drag, and weight (gravity). The force of weight (gravity) depends on the mass of the UAV and the gravitational acceleration. In the case of UAVs, the mass is constant during flight, and the change in gravitational acceleration due to the change in altitude is negligible. Lift and aerodynamic drag depend on the airspeed, pressure, temperature, ambient density, and aerodynamic coefficients of the aircraft.

The aerodynamic coefficients of UAVs are derived from the geometric dimensions of the UAVs. The thrust depends on the characteristics of the power unit, the shape and size of the propeller, and the environment in which it operates. The position angles are an important factor when calculating UAV forces. Using position angles can transform the individual components of forces and moments into a common system. In our case, we used the aircraft coordinate system. When describing the translational motion of UAVs, we began with the equation of aerodynamic forces. Aerodynamic forces are generated on the lifting aerofoil area and tail surfaces [22]. The calculation of aerodynamic forces is described by the following relations:

$$F_{x\_aero} = -((C_{x\alpha} \cdot \alpha) + C_{x0}) \cdot W_{surf} \cdot q_{bar},$$

$$F_{y\_aero} = \left(\beta \cdot C_{y\beta} + \left(\frac{C_{yr} \cdot r \cdot W_{span}}{2 \cdot V_{aero}}\right) + C_{y\Delta RUD} \cdot \Delta RUD\right) \cdot W_{surf} \cdot q_{bar},$$

$$F_{z\_aero} = \left(C_{z0} + C_{z\alpha} \cdot \alpha + \left(\frac{C_{zq} \cdot q \cdot W_c}{V_{aero}}\right) + C_{z\Delta EL} \cdot \Delta EL\right) \cdot W_{surf} \cdot q_{bar},$$

$$(1)$$

where

F_{x_aero}: Aerodynamic force acting on the aircraft X-axis,

C_{x_α}: Aerodynamic coefficient expressing the dependence of drag on angle α,

α: Angle of attack,

C_{x_0}: Aerodynamic coefficient expressing the dependence of drag on angle $\alpha = 0$,

W_{surf}: Wing surface,

q_{bar}: Total atmospheric pressure (dynamic pressure),

F_{y_aero}: Aerodynamic force acting on the aircraft Y-axis,

β: Sideslip angle,

C_{y_β}: Aerodynamic coefficient expressing dependence on lateral force β,

C_{y_r}: Aerodynamic coefficient expressing dependence on lateral force r,

r: Angular speed of rotation around the Z-axis in the plane coordinate system,

W_{span}: Wing span,

V_{aero}: Indicated air speed,

$C_{y\_\Delta RUD}$: Aerodynamic coefficient expressing the dependence of the yaw moment,

ΔRUD: Vertical control surface (rudder) deflection,

F_{z_aero}: Aerodynamic force acting on the aircraft Z-axis,

C_{z_0}: Aerodynamic coefficient expressing the dependence of lift on angle $\alpha = 0$,

C_{z_α}: Aerodynamic coefficient expressing the dependence of lift on angle α,

C_{z_q}: Aerodynamic coefficient expressing the dependence of q,

q: Angular speed of rotation around the Y-axis in the plane coordinate system,

W_c: Wing chord,

$C_{z\_\Delta EL}$: Aerodynamic coefficient expressing the dependence of the pitch moment,

ΔEL: Horizontal control surface (elevator) deflection.

The constants in the equations are the aerodynamic coefficients of the aircraft denoted by c and the geometric dimensions of the wings as the wingspan, wing area, and center of the wing chord (W_{span}, W_{surf}, and W_c, respectively).

The UAV variables are angle of attack α, dynamic pressure q_{bar}, airspeed V_{aero}, horizontal control surface (elevator), and vertical control surface (rudder) deviations ΔEL and ΔRUD. All the forces are situated in the aerodynamic coordinate system. We created the change in the UAV position with moments using control surfaces.

The aerodynamic moments in the individual axes of a UAV are described by the following relations [23]:

$$L_{aero} = \left[C_{l\Delta RUD} \cdot \Delta RUD + C_{l\Delta AIL} \cdot \Delta AIL + C_{l\beta} \cdot \beta + \left(\frac{C_{lp} \cdot p \cdot W_{span}}{2 \cdot V_{aero}}\right) + \left(\frac{C_{lr} \cdot r \cdot W_{span}}{2 \cdot V_{aero}}\right)\right] \cdot W_{surf} \cdot W_{span} \cdot q_{bar},$$

$$M_{aero} = \left[C_{m\Delta EL} \cdot \Delta EL + C_{m\alpha} \cdot \alpha + C_{m0} + \left(\frac{C_{mq} \cdot q \cdot W_c}{V_{aero}}\right)\right] \cdot W_{surf} \cdot W_c \cdot q_{bar},$$

$$N_{\text{aero}} = \left[C_{n\Delta\text{AIL}} \cdot \Delta\text{AIL} + C_{n\Delta\text{RUD}} \cdot \Delta\text{RUD} + C_{n\beta} \cdot \beta + \left(\frac{C_{np} \cdot p \cdot W_{\text{span}}}{2 \cdot V_{\text{aero}}} \right) \right.$$
$$\left. + \left(\frac{C_{nr} \cdot r \cdot W_{\text{span}}}{2 \cdot V_{\text{aero}}} \right) \right] \cdot W_{\text{span}} \cdot W_{\text{surf}} \cdot q_{\text{bar}}, \tag{2}$$

where

L_{aero}: Rotation moment around X-axis,

$C_{l\_\Delta\text{RUD}}$: The aerodynamic coefficient expressing the roll moment dependence on ΔRUD,

$C_{l\_\Delta\text{AIL}}$: The aerodynamic coefficient expressing the roll moment dependence on ΔAIL,

ΔAIL: Aileron deflection,

C_{l_β}: Coefficient expressing the roll moment dependence on β,

C_{l_p}: Coefficient expressing the roll moment dependence on p,

C_{l_r}: Coefficient expressing the roll moment dependence on r,

p: Angular speed of rotation around the X-axis in the plane coordinate system,

M_{aero}: Rotation moment around the Y-axis,

$C_{m\_\Delta\text{EL}}$: The aerodynamic coefficient expressing the pitch moment dependence on ΔEL,

ΔEL: The aerodynamic coefficient expressing the pitch moment dependence on ΔEL,

C_{m_α}: The aerodynamic coefficient expressing the pitch moment dependence on α,

C_{m_0}: The aerodynamic coefficient expressing the pitch moment dependence on $\alpha = 0$,

C_{m_q}: The aerodynamic coefficient expressing the pitch moment dependence on q,

N_{aero}: Rotation moment around the Z-axis,

$C_{n\_\Delta\text{AIL}}$: Aerodynamic coefficient expressing the turning moment dependence ΔAIL,

$C_{n\_\Delta\text{RUD}}$: Aerodynamic coefficient expressing the turning moment dependence ΔRUD,

C_{n_β}: Aerodynamic coefficient expressing the turning moment dependence β,

C_{n_p}: Aerodynamic coefficient expressing the turning moment dependence p,

C_{n_r}: Aerodynamic coefficient expressing the turning moment dependence r.

The longitudinal motion of UAVs is described by a set of four first-order linear differential equations with four unknowns $x_{\text{lon}} = [u, w, q, \theta]^T$. The equations are related to the axes of the coordinate system firmly connected to the aircraft. The longitudinal motion of UAV is described by the motion equations corresponding to the forces X and Z and the moment M. Movements that are not limited in the longitudinal plane have no effect, i.e., "$v = p = r = $ lateral angles"…"$= 0$" [24].

The following relationship is used to describe the system in the state space:

$$\dot{x}_{\text{lon}} = A_{\text{lon}} x_{\text{lon}} + B_{\text{lon}} \delta_e. \tag{3}$$

The notation of linear differential equations for the longitudinal motion of the UAV has the following form [25]:

$$\dot{x}_{\text{lon}} = \begin{pmatrix} x_u & x_w & x_q - w_e & -g\cos\theta_e \\ z_u & z_w & z_q + u_e & -g\sin\theta_e \\ m_u & m_w & m_q & 0 \\ 0 & 0 & 1 & 0 \end{pmatrix} \begin{pmatrix} u \\ w \\ q \\ \theta \end{pmatrix} + \begin{pmatrix} x_{\delta_e} \\ z_{\delta_e} \\ m_{\delta_e} \\ 0 \end{pmatrix} (\delta_e). \tag{4}$$

The root shape of the characteristic equation determines the properties of the UAV's motion. Depending on the coefficient values of the characteristic equation, which determine the aerodynamic and inertial characteristics of the UAV, it is possible to determine variants of the UAV's motion from the graphical solution of differential equations. The longitudinal motion of the UAV is characterized by two complex associated roots, and the motion of the UAV is described by two oscillating members, the short-period and phugoid modes.

We observed the static and dynamic stability of UAVs. With static stability, when the UAV deviates from the equilibrium position, the UAV returns spontaneously to the equilibrium position without mechanical or human intervention. In the longitudinal plane with a dynamically stable UAV, the amplitude of the oscillations will decrease with external intervention until it reaches a stable value.

2.2. Modelling the Noise of UAV Sensors. In hobby-type UAVs, it is not effective to install expensive and large INS sensors. It is therefore necessary to analyse the output of the IMU sensors or take steps to increase the accuracy of the measurement. These MEMS sensors are more susceptible to the different types of noise that can be registered in the sensor.

For reliable analysis of the noise mechanisms of the IMU inertial sensors, it is necessary to perform static measurements over a long-time interval. The Allan variation method can be used for the analysis of UAV sensors [15]. The use of Allan variance for the analysis of IMU sensors is determined by the IEEE standard, which defines the procedure of steps by which the results are analysed. The result of the analysis is the representation of noise in the output of the IMU sensors in terms of long-term time development [26].

To create an Allan variance graph, it is necessary to sample a continuous time series. It is defined by the sampling frequency f_s, which is already defined before the start of the static measurement. The total number of samples is defined by the following relation:

$$N = f_s T. \tag{5}$$

In equation (5), T represents the time of the entire measurement series in seconds. After subsequent sampling of this continuous signal, the Allan variance calculation process is as follows:
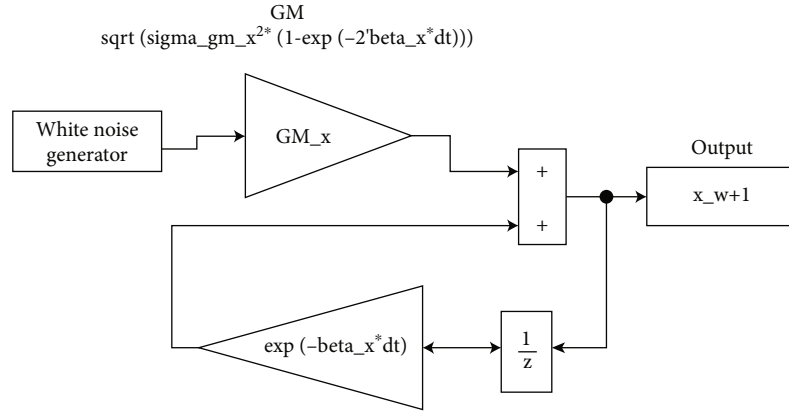
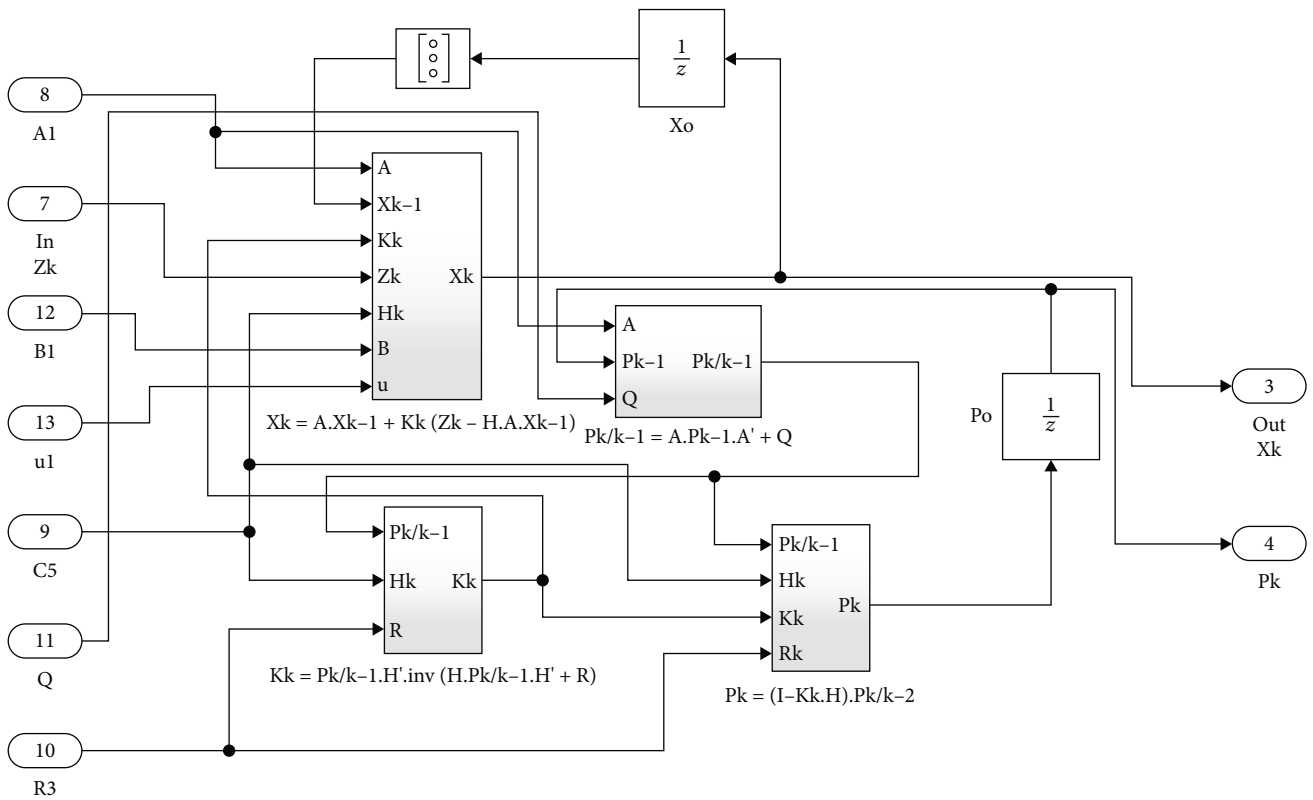FIGURE 1: Bias drift modelled as a first-order Gauss-Markov process.

FIGURE 2: Discrete linearized Kalman filter model in Matlab/Simulink.

A vector of averaged intervals τ_{AV} in seconds is created.

$$\tau_{AV} \left[1\, 2\, \cdots\, \frac{T}{2} \right]. \quad (6)$$

For each vector τ_{AV}, the time series $a(t)$ is divided into M clusters.

$$M(\tau_{AV}) = \frac{T}{\tau_{AV}}. \quad (7)$$

The average $a(t)$ is then calculated for each cluster M:

$$\bar{a}(\tau_{AV}, k) = \frac{1}{L} \sum_{i=1}^{L} a_i, \ L = f_s . \tau_{AV}, \ k = [1\, 2\, \cdots\, M(\tau_{AV})]. \quad (8)$$

Using the Allan variance $\sigma^2(\tau_{AV})$ the output for the individual cluster averages of vectors is the averaged interval τ_{AV} according to the following relation:

$$\sigma^2(\tau_{AV}) = \frac{1}{2(K-1)} \sum_{k=1}^{K-1} (\bar{a}_{k+1}(L) - \bar{a}_k(L))^2. \quad (9)$$

TABLE 1: The UAV's aerodynamic coefficient values obtained by simulation.

Effects		Shortcut	Dependency on variable	Value
Aerodynamic coefficients of forces	Axis Z	C_{L_α}	Dependency of lift on α	4.56
		$C_{L\_\alpha 0}$	Dependency of lift on $\alpha = 0$	0.51
		$C_{L\_\Delta EL}$	Dependency of lift on ΔEL	-0.85
		CL_q	Dependency of lift on q	7.2
	Axis X	C_{D_α}	Dependency of drag on α	0.39
		$C_{D\_\alpha 0}$	Dependency of drag on $\alpha = 0$	0.03
	Axis Y	C_{Y_β}	Dependency of side force on β	-0.18
		C_{Y_r}	Dependency of side force on r	0.314
		$C_{Y\_\Delta RUD}$	Dependency of side force on ΔRUD	0.2
Aerodynamic coefficients of moments	Axis X	$C_{l\_\Delta RUD}$	Dependency of roll moment on ΔRUD	0.004
		$C_{l\_\Delta AL}$	Dependency of roll moment on ΔAL	-0.1
		C_{l_β}	Dependency of roll moment on β	0.012
		C_{l_p}	Dependency of roll moment on p	-0.32
		C_{l_r}	Dependency of roll moment on r	0.028
	Axis Y	$C_{m\_\Delta EL}$	Dependency of pitch moment on ΔEL	-2.442
		C_{m_q}	Dependency of pitch moment on q	-48
		C_{m_α}	Dependency of pitch moment on α	-1.13
		$C_{m\_\alpha 0}$	Dependency of pitch moment on $\alpha = 0$	-0.04
	Axis Z	C_{n_r}	Dependency of yaw moment on r	-0.09
		C_{n_p}	Dependency of yaw moment on p	-0.07
		$C_{n\_\Delta AL}$	Dependency of yaw moment on ΔAL	-0.12
		$C_{n\_\Delta RUD}$	Dependency of yaw moment on ΔRUD	-0.04
		C_{n_β}	Dependency of yaw moment on β	0.089

For the analysis of IMU noise in the time domain, a graph is created in a logarithmic scale, where it is an independent variable τ_{AV} and a dependent variable $\sigma^2(\tau_{AV})$.

To correctly model the error model according to the standard, it is necessary to determine the bias drift correlation time, the bias drift standard deviation, and the broadband noise standard deviation.

Bias drift is modelled as a first-order Gauss-Markov process. These parameters can be determined using the Allan variation and appropriate relationships. The standard deviation of the wideband noise is defined by the standard as a line with a slope of $-1/2$. Its range can be determined by the following relationship:

$$\sigma_{RW} = \frac{N_{AV}}{\sqrt{\Delta t}}, \tag{10}$$

where N_{AV} is the wideband noise coefficient and Δt is the sample time.

The point in the Allan variation graph at which the curve reaches the local maximum is used to determine the bias drift correlation time. The definition of correlation time is based on the following relationship:

$$\tau_{AC} = 1.89 T_C. \tag{11}$$

There is a quick direct approach for extraction of the N and B noise parameters that does not require least mean square estimation procedure.

To determine the bias instability of the sensors, a coefficient B is used, which is calculated according to the following relation:

$$N = \frac{\sigma_{A(\tau_R)}\sqrt{\tau_R}}{60} \; (\text{deg/hr}),$$
$$B = \frac{\sigma_{A(\tau_B)}}{0,664} \; (\text{deg}). \tag{12}$$

τ_R and τ_B represent the time on the root AVAR versus τ, graph where the parameters N and B are to be evaluated.

In analysing UAV sensor errors, it is also necessary to determine the misalignment error and the nonorthogonality error. These errors must be included in the sensor error model.

When we model bias drift as a first-order Gauss-Markov process, we can describe its behaviour as follows:

$$x_{n+1} = e^{-\beta\Delta t}.x_n + \sqrt{\sigma_{GM}^2\left(1 - e^{-2\beta\Delta t}\right)}.w_n. \qquad (13)$$

We calculate the constant β according to the following relation:

$$\beta = \frac{1}{T_C}, \qquad (14)$$

where T_C is calculated as follows:

$$T_C \approx \frac{T}{1,89}, \qquad (15)$$

where T_C is the correlation time and the numerical value of T is read from the Allan variance graph at the point of overshoot of the curve (local maximum).

For calculation, the previous sample x_n, white noise w_n, and constants β, Δt, and σ_{GM} are used. Constant Δt represents the sampling time. The value of the constant σ_{GM} is equal to the standard deviation of the filtered signal. Constant β is calculated as the inverse of the known value of correlation time T_C.

If the first-order relationship describing the Gauss-Markov process is known, then a simulation scheme in Matlab/Simulink can be created to simulate the effect of bias drift on sensor measurements. The basis for simulating the Gauss-Markov process is a white noise generator. The model representing the sensor bias drift is shown in Figure 1. Another noise mechanism like angle random walk (ARW) affecting sensor measurement needs to be modelled. White noise generator block is used to simulate ARW noise. In the field that determines the power of the generator, we insert the square of the N value obtained from the Allan graph.

To determine the sensor misalignment, we used the following relationship:

$$\underline{\omega}_{C,B}^D = \left[I_3 + \Delta E_B^D \times\right].\underline{\omega}_{C,B}^B, \qquad (16)$$

where $\underline{\omega}_{C,B}^D$ is the misalignment error, I_3 is the unit matrix, $\Delta E_B^D \times$ is the antisymmetric matrix of deviations in the individual axes, and $\underline{\omega}_{C,B}^B$ is the input angular velocities of the gyroscopes in the axes (body frame) of the aircraft.

To model the nonorthogonality error, we began with the following relation:

$$\underline{\omega}_{C,B}^i = \left[I_3 + \Delta E_B^i \times\right].\underline{\omega}_{C,B}^D, \qquad (17)$$

where $\underline{\omega}_{C,B}^i$ is the error of gyroscope nonorthogonality and $\Delta E_B^i \times$ is the antisymmetric matrix of deviations in the individual axes (INS, body frame).

2.3. Atmospheric Disturbances Affecting UAVs. The overall stability of UAV control is influenced by the atmosphere in the environment in which the aircraft flies. The moments

TABLE 2: VRW and ARW sensor values of the Pixhawk PX4 control unit.

Sensor axis		Calculation using the Allan variation graph
Accelerometer (m/s)	X	1.3044^*10^{-2} (m/s)
	Y	1.3835^*10^{-2} (m/s)
	Z	1.5381^*10^{-2} (m/s)
Gyroscope (°/s)	X	7.9778^*10^{-4} (°/s)
	Y	7.2051^*10^{-4} (°/s)
	Z	7.6183^*10^{-4} (°/s)

TABLE 3: Autocorrelation τ_{AC} and correlation time τ_C of IMU sensors.

Sensor axis		τ_{AC} (s)	T_C (s)
Accelerometer (m/s)	X	772.1 (s)	408.52 (s)
	Y	725.6 (s)	383.92 (s)
	Z	710.8 (s)	376.08 (s)
Gyroscope (°/s)	X	700.9 (s)	370.85 (s)
	Y	725.4 (s)	383.81 (s)
	Z	730 (s)	386.24 (s)

TABLE 4: Drift bias size for individual IMU UAV sensor axes.

Sensor axis		Drift bias value
Accelerometer (m/s)	X	3.0571^*10^{-4} (m/s)
	Y	7.9462^*10^{-5} (m/s)
	Z	2.9856^*10^{-6} (m/s)
Gyroscope (°/s)	X	8.0532^*10^{-3} (°/s)
	Y	6.8521^*10^{-3} (°/s)
	Z	1.2557^*10^{-3} (°/s)

caused by horizontal and vertical airflow are fundamental disturbances that affect the UAVs during flight and the landing phase [27].

Turbulence denotes changes in atmospheric motion that disrupt flight, especially during take-off and landing. Turbulence can arise from changes in atmospheric pressure or hot or cold fronts. The instantaneous velocity vector changes randomly within certain limits, changing its size and direction.

Due to the complexity, simplified models were used for simulation and description of Dryden's turbulence model. In Dryden's turbulence model, the components of the linear and angular velocities of continuous impacts are spatially changing stochastic processes.

Noise with known spectral properties such as velocity and angular velocity deviation in individual aircraft axes is used for modelling. The noise spectrum for each of the disturbances is defined by the turbulence length L, the air velocity V, and the turbulence intensity σ.
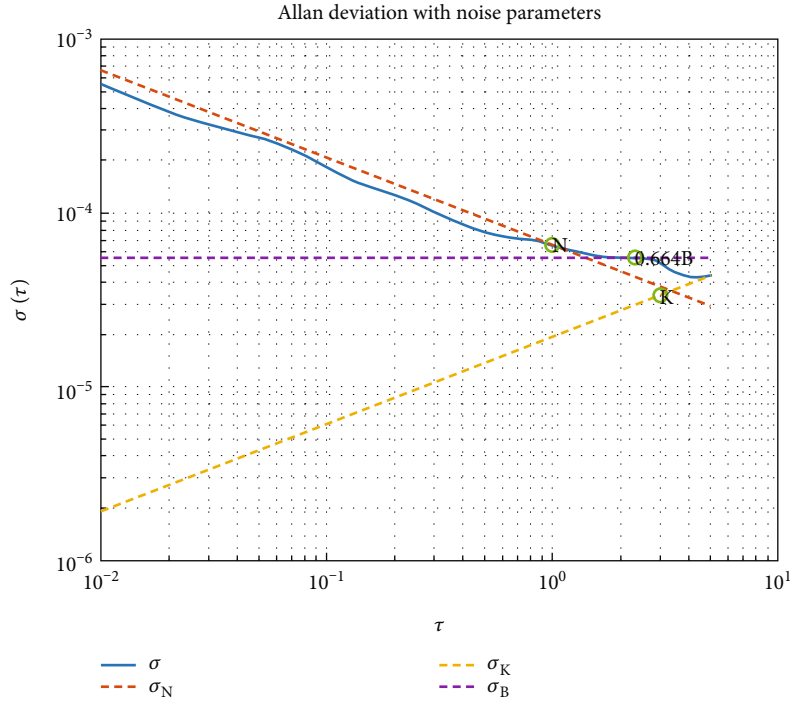
FIGURE 3: Analysis of noise mechanisms on the gyroscope in the Y-axis using the Allan variation.
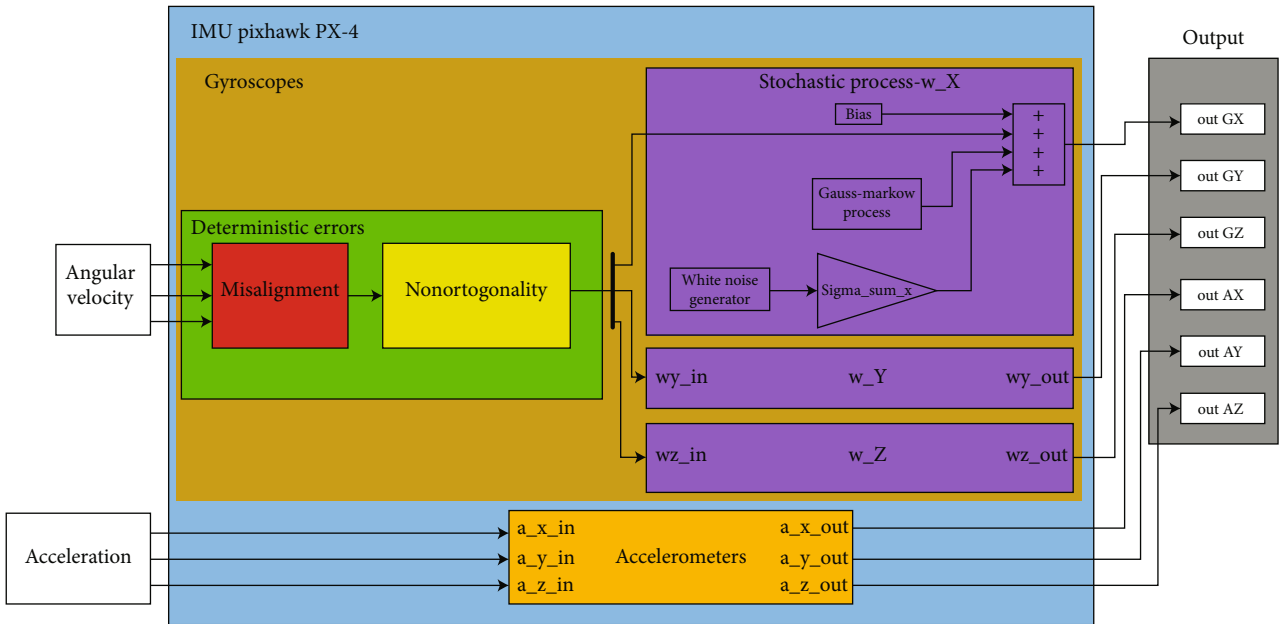

FIGURE 4: IMU Pixhawk PX-4 sensor error model constructed using Matlab/Simulink.

The turbulence rate length is the length of the turbulent field expressed in the longitudinal, lateral, and vertical axes (L_u, L_v, and L_w, respectively).

The turbulence intensity is the magnitude of turbulence expressed in the longitudinal, lateral, and vertical axes (σ_u, σ_v, and σ_w, respectively); it is given in ft/s or m/s.

To overcome the UAV turbulence, the time T is required:

$$T = \frac{L}{V}. \tag{18}$$

The UAV experiences a turbulent wave with a frequency of

$$\omega = \frac{2\pi}{T} = \frac{2\pi}{L/V}. \tag{19}$$

Dryden's turbulence model is characterized by the power spectral density Φ as a function of frequency.
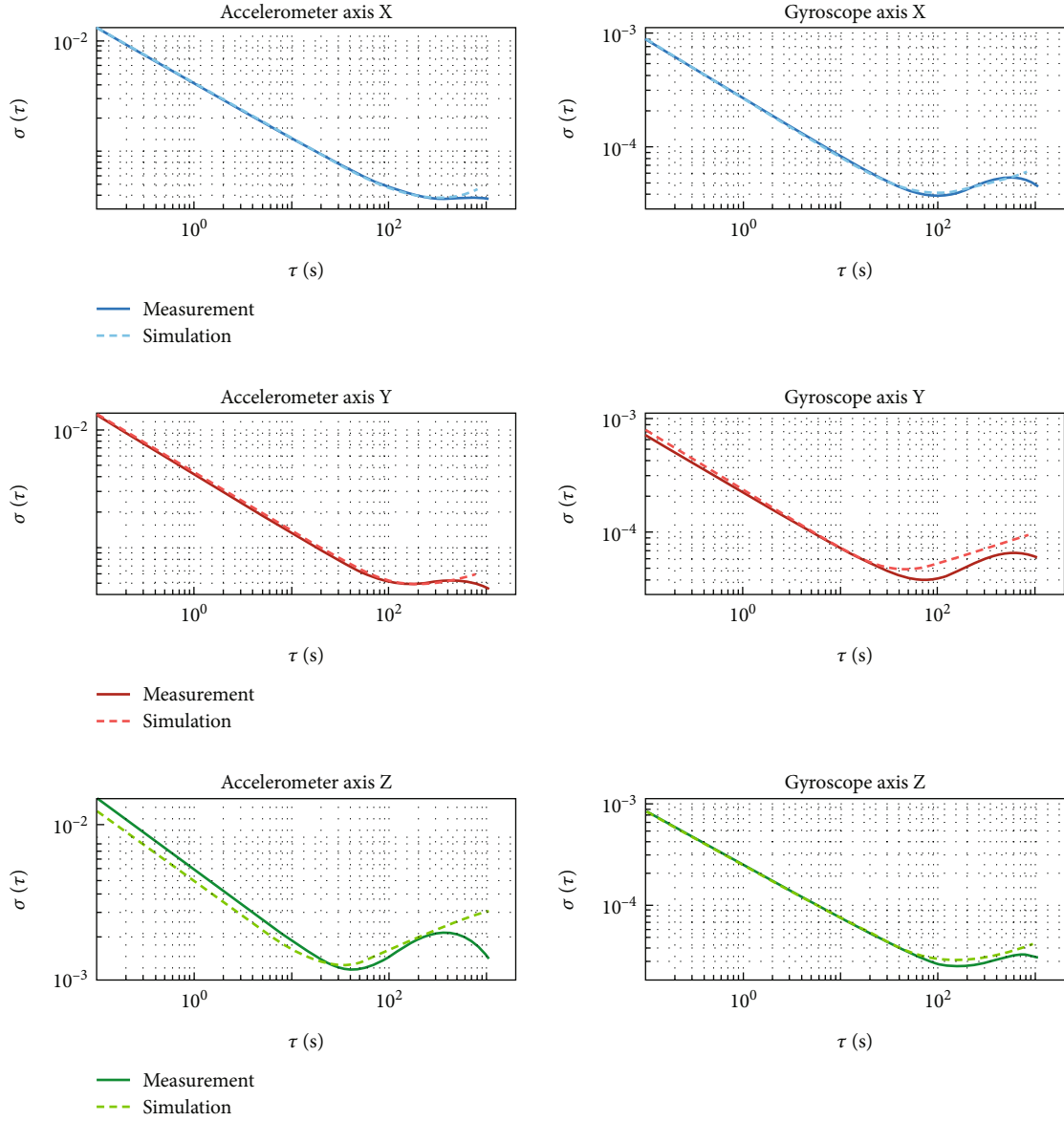
FIGURE 5: Analysis of measured and simulated sensor data using the Allan variation and the generated IMU error model.

The power spectral density for the linear flow velocity components (u_g, v_g, and w_g) has the following form:

$$\Phi_u(\omega) = \frac{2\sigma_u^2 L_u}{\pi V} \frac{1}{1 + (L_u(\omega/V))^2},$$

$$\Phi_v(\omega) = \frac{2\sigma_v^2 L_v}{\pi V} \frac{1 + 12(L_v(\omega/V))^2}{\left[1 + 4(L_v(\omega/V))^2\right]^2}, \qquad (20)$$

$$\Phi_w(\omega) = \frac{2\sigma_w^2 L_v}{\pi V} \frac{1 + 12(L_w(\omega/V))^2}{\left[1 + 4(L_w(\omega/V))^2\right]^2}.$$

The power spectral density for the angular flow velocity components (p_g, q_g, and r_g) has the following form:

$$\Phi_p(\omega) = \frac{\sigma_w^2}{V L_w} \frac{0,8(2\pi L_w/4b)^{1/3}}{1 + (4b\omega/\pi V)^2},$$

$$\Phi_q(\omega) = \frac{\pm(\omega/V)^2}{1 + (4b\omega/\pi V)^2} \Phi_w(\omega), \qquad (21)$$

$$\Phi_r(\omega) = \frac{\pm(\omega/V)^2}{1 + (3b\omega/\pi V)^2} \Phi_v(\omega),$$

where b is the wingspan of the UAV.

Wind shear is defined as a change in wind speed and direction at a relatively short distance from the atmosphere. The wind, by its action, introduces an error component into the measurement of UAV sensors. A sudden gust of wind acting on the UAV from below results in an increase in the
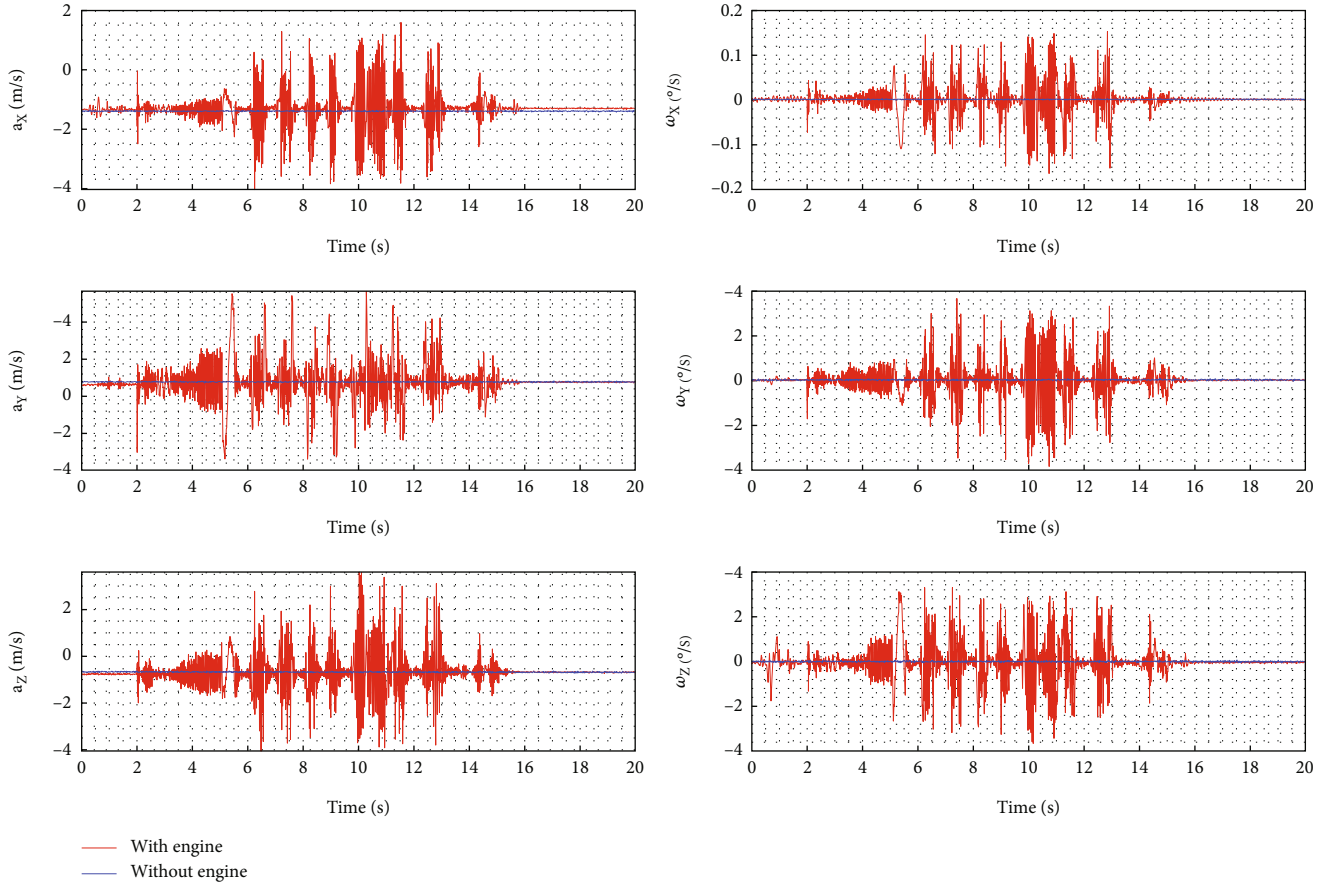
FIGURE 6: The course of the UAV motor's influence on the measurement of individual IMU sensors.

angle of attack and a change in the airspeed vector relative to the ground.

The UAV "Skydog" uses an electric noncontact AC (alternating current) motor with rotating housing and neodymium magnets for forward movement, which introduces a certain component of the error into the measurement process.

2.4. Design and Implementation of Kalman Filter.
The Kalman filter method can be an effective and versatile method of combining the outputs of IMU sensors that are loaded with various noise mechanisms and disturbances to estimate the states of a system that has indeterminate dynamics. The basic parts defined by the Kalman filter are the state vector and its covariance, the system model, the measurement vector and its covariance, and the measurement model.

When used in UAV control and navigation, the state vector contains position-determining components or errors in position. The Kalman filter also contains estimates of angular position, velocities, and errors of individual IMU UAV sensors. The covariance matrix of the state vector defines the uncertainties in the state estimates of the Kalman filter and the degree of correlation between the errors of the estimates [28].

The state estimate can be considered optimal if the sum of squared errors of the estimated state variables is as small as possible at any time.

To use the UAV model with the optimal Kalman filter, it is necessary to create a state space of the UAV model in the discrete form [29].

Discrete state space is characterized by the following relationships:

$$x_{k+1} = A_D x_k + B_D u_k + G w_k,$$
$$y_{k+1} = C_D x_{k+1} + D_D v_{k+1}, \tag{22}$$

where x_{k+1} is the n-dimensional state vector, y_{k+1} is the m-dimensional measurement vector, v_{k+1} is the m-dimensional measurement error vector (Gaussian white noise), u_k is the input signal, w_k is an n-dimensional Gaussian white noise with zero mean, A_D is a system matrix of $n \times n$, B_D is an excitation matrix of $n \times m$, C_D is an output matrix of $m \times n$, D_D is the direct feedback matrix bonds, and $k = 1, 2, 3, \cdots$ is the sample number.

To update the estimated state vector, we used the following relation:

$$\hat{x}_k = \hat{x}_{k,k-1} \Phi_{k-1} + K_k \cdot [y_k - H \cdot \hat{x}_{k,k-1}]. \tag{23}$$
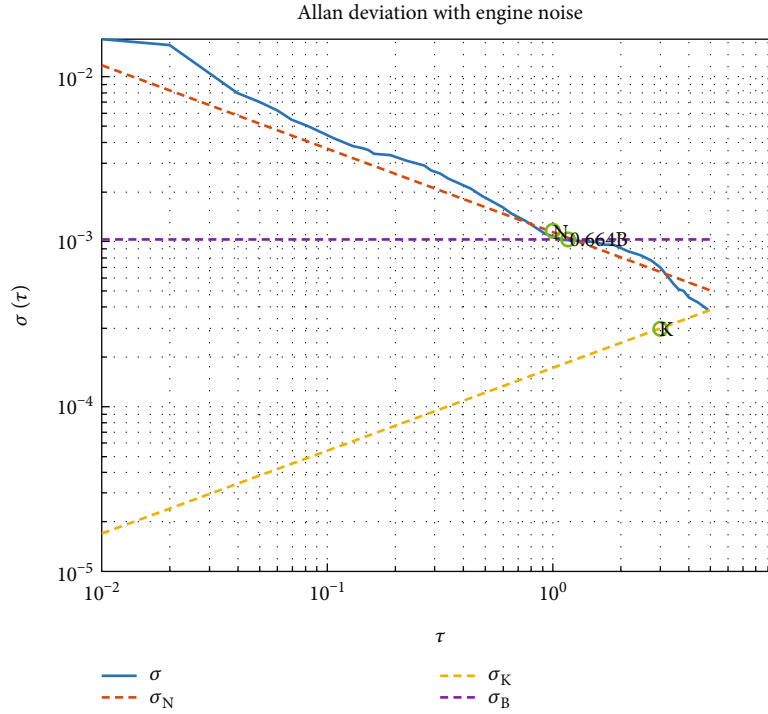
FIGURE 7: Analysis of the motor effect on the gyroscope in the Y-axis using the Allan variation.

To calculate the matrix gain (weight matrix), the following relation is used:

$$K_k = P_{k,k-1} \cdot H_k^T \cdot \left(H_k \cdot P_{k,k-1} \cdot H_k^T + R_k\right)^{-1}. \quad (24)$$

To update the covariance matrix, the following relationship is used:

$$P_k = (I - K_k \cdot H_k) \cdot P_{k,k-1} \cdot (I - K_k \cdot H_k)^T + K_k \cdot R_k \cdot K_k^T, \quad (25)$$

where $\hat{x}_{k-1}$ is the corrected value of the estimated state vector from the previous state of the algorithm, Φ_{k-1} is the discrete matrix of the dynamical system, $\hat{x}_{k,k-1}$ is the predicted value of the estimated state vector, K_k is the gain matrix, H_k is the measurement matrix, R_k is the covariance measurement matrix, y_k is the current measurement vector, $\hat{x}_k$ is the updated value of the estimated state vector, P_k is the updated value of the estimated covariance, and Q_k is the covariance matrix of the process noise.

It is assumed that the noises w_k and v_k are white noises with zero mean value [29].

The mean and covariance of the random processes are described by

$$E\langle w_k \rangle = 0, E\langle w_k w_i^T \rangle = Q_k \cdot \Delta(k-i),$$
$$E\langle v_k \rangle = 0, E\langle v_k v_i^T \rangle = R_k \cdot \Delta(k-i), \quad (26)$$

where w_k is the process noise vector and v_k is the measurement noise vector, shown in Figure 2.

TABLE 5: Standard deviation values of the noise introduced into the measurement by the UAV engine.

Sensor axis		σ_{VM}
	X	0.0547927
Accelerometer (m/s)	Y	0.0495273
	Z	0.0741763
	X	0.0032016
Gyroscope (°/s)	Y	0.0017807
	Z	0.0020208

3. Results and Discussion

The values of the forces and moments acting on the UAV "Skydog" affected the geometric and aerodynamic coefficients. The necessary geometric coefficients for the calculation of the forces and moments of the UAV were obtained from the technical documentation and by measuring the aircraft itself. Aerodynamic coefficients for the UAV "Skydog" were obtained using the XFLR5 program. Their values are given in Table 1 [30].

Based on the obtained aerodynamic coefficients shown in Table 1, a mathematical simulation model of the dynamic movement UAV "Skydog" was created. To verify it, a longitudinal plane comparison was performed [31].

When designing an optimal regulator for the motion control of the UAV "Skydog," a control model scheme from the UAV transfer function expressed the response of the aircraft in pitch rate to elevator deflection, PID pitch rate
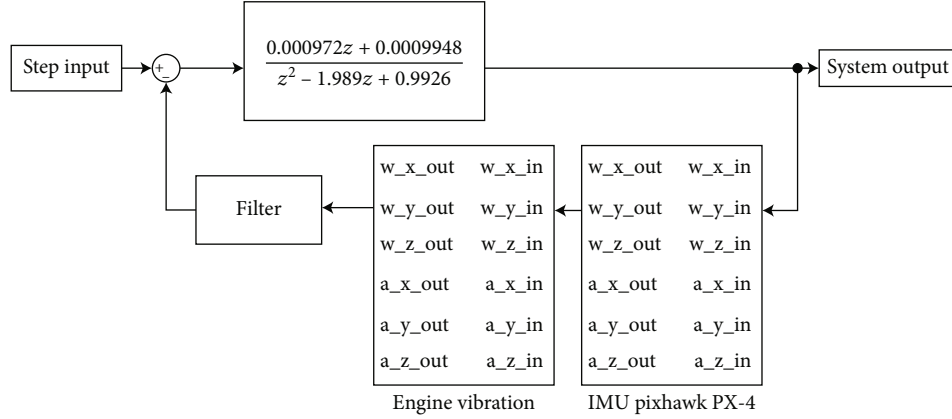
FIGURE 8: Implemented filter into the UAV control system.

controller, and the actuator transfer function [29]. Based on the knowledge of the approximation polynomials, the PID controller coefficients for the selected UAV "Skydog" speed were calculated. The best PID gains obtained by tuning were $K_p = 10.25$, $K_i = 65.12$, $K_d = 0.898$; and filter coefficient is $N = 0.002666$ [29].

The controller with these coefficients was then used to create a state space model of the Skydog airplane with the PID controller in a feedback loop. The observed state parameter $\dot{x}_1$ represents the pitch rate $-q$.

$$\begin{pmatrix} \dot{x}_1 \\ \dot{x}_2 \\ \dot{x}_3 \\ \dot{x}_4 \end{pmatrix} = \begin{pmatrix} -1.003*10^4 & 1 & 0 & 0 \\ -2.474*10^5 & 0 & 1 & 0 \\ -1.619*10^6 & 0 & 0 & 1 \\ -6.944*10^5 & 0 & 0 & 0 \end{pmatrix} \begin{pmatrix} x_1 \\ x_2 \\ x_3 \\ x_4 \end{pmatrix} + \begin{pmatrix} 9654 \\ 2.457*10^5 \\ 1.618*10^6 \\ 6.944*10^5 \end{pmatrix} (q_{cmd}),$$

$$(27)$$

$$C_{90} = \begin{bmatrix} 1 & 0 & 0 & 0 \end{bmatrix}, \tag{28}$$

$$D_{90} = [0]. \tag{29}$$

The UAV "Skydog" model for a speed of 90 km/h in a discreet time with a sampling rate of 100 Hz has the form of matrixes A (30) and B (31), and the state variable $\dot{x}_1$ represents the pitch rate $-q$. It is the observed parameter of the model; matrixes C and D are the same as (28) and (29):

$$A_{D90} = \begin{bmatrix} -0.002058 & -7.575*10^{-5} & 8.752*10^{-7} & 4.515*10^{-9} \\ -20.61 & -0.7762 & 0.008858 & 4.618*10^{-5} \\ -126.2 & -1.42 & -0.9927 & -0.009975 \\ -53.87 & -0.6078 & -0.003135 & 1 \end{bmatrix},$$

$$(30)$$

$$B_{D90} = \begin{bmatrix} 0.9711 \\ 90.63 \\ 672.2 \\ 289.8 \end{bmatrix}. \tag{31}$$

The resulting output of this representation of the UAV in longitudinal plane of motion is the pitch rate q as a response to the commanded pitch rate q_{cmd}.

The UAV Pixhawk control unit is a programmable platform; it contains SCA3100-D04 accelerometers and IDG-500 gyroscopes for the X- and Y-axes and an ISZ-500 gyroscope for the Z-axis.

For the analysis of IMU sensors, a static measurement was performed with zero effect of external forces. The Allan variation method was used to define and eliminate the noise mechanisms of the sensors. The specified velocity random walk (VRW) and angle random walk (ARW) values for the accelerometers and gyroscopes of the Pixhawk control unit are given in Table 2, for a sampling time of Δt 0.1 seconds, N gyroscope for Y axe $2.278*10^{-4}$.

Where N is the broadband noise coefficient, B is the bias instability coefficient, K is the random walk coefficient.

The determined values of the autocorrelation τ_{AC}, correlation time τ_C, and drift bias of IMU sensors are given in Tables 3 and 4.

The Allan variation method was used to define and remove noise IMU mechanisms. Figure 3 shows graphs of the Allan variation of individual accelerometer axes and IMU gyroscopes. A sensor error model was compiled using Matlab/Simulink, which included blocks for modelling noise mechanisms, nonorthogonality errors, and IMU Pixhawk PX4 sensor misalignment errors, shown in Figure 4.

The internal structure of the error model for accelerometers and gyroscopes is the same, and the output is different only in the measured units.

Using the Allan variation, the output waveforms from the measured IMU UAV sensor data and the data from the generated IMU error model were compared, shown in Figure 5.

The IMU fault model includes the simulation of noise introduced into the measurement of sensors with the engine influence. The UAV "Skydog" uses an electric noncontact AC motor with rotating housing and AXI 5320/34 neodymium magnets for forward movement. The motor is powered and controlled by the regulator SPIN 77 opto, which serves to regulate the voltage and current to the motor depending on the required power from the pilot. The regulator is powered by FOXY G2 onboard batteries with a voltage of 18.5 V
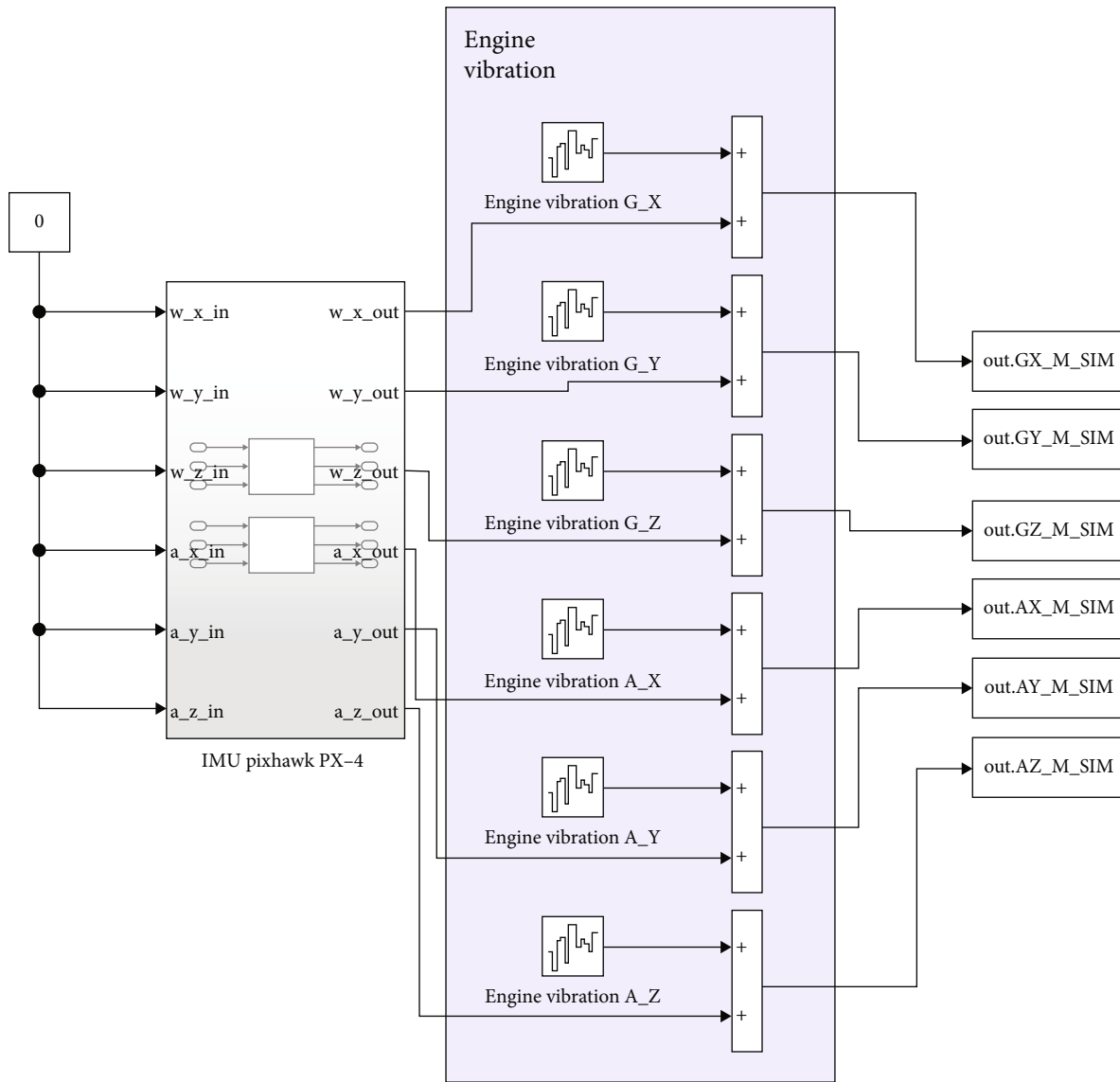
Figure 9: Engine vibration simulation model.

Table 6: Values of the coefficients of the designed filter.

a_0	a_1	a_2	b_0	b_1	b_2
0.02008	0.04017	0.02008	1	-1.561	0.6414

and a capacity of 5000 mAh. The effect of the motor on the IMU UAV sensors was simulated as white noise. The magnitude of the interference is proportional to the standard deviation of the noise measured during the static measurement of the motor influence on the measurement of the IMU sensors, shown in Figures 6 and 7. The standard deviation values of the noise are shown in Table 5.

To reduce the impact of the motor on the IMU UAV sensors, a filter was designed, which was implemented using the "digital filter design" block, Figure 8, in the Matlab/Simulink program environment. A low-pass Butterworth IIR filter was designed as optimal, shown in Figure 9.

The coefficients of the designed filter have the following values listed in Table 6.

For better information about the functioning of the designed filter, the basic parameters of the signal were therefore evaluated, namely, mean value, standard deviation, median, and variance. The result from the simulation is shown in Figure 10. These values for all three axes of the accelerometer are shown in Table 7.

The atmospheric impact model was based on the "Dryden wind turbulence model" block in the Matlab/Simulink environment. The inputs of this block were airplane flight speed, airplane flight altitude, and cosine control matrix
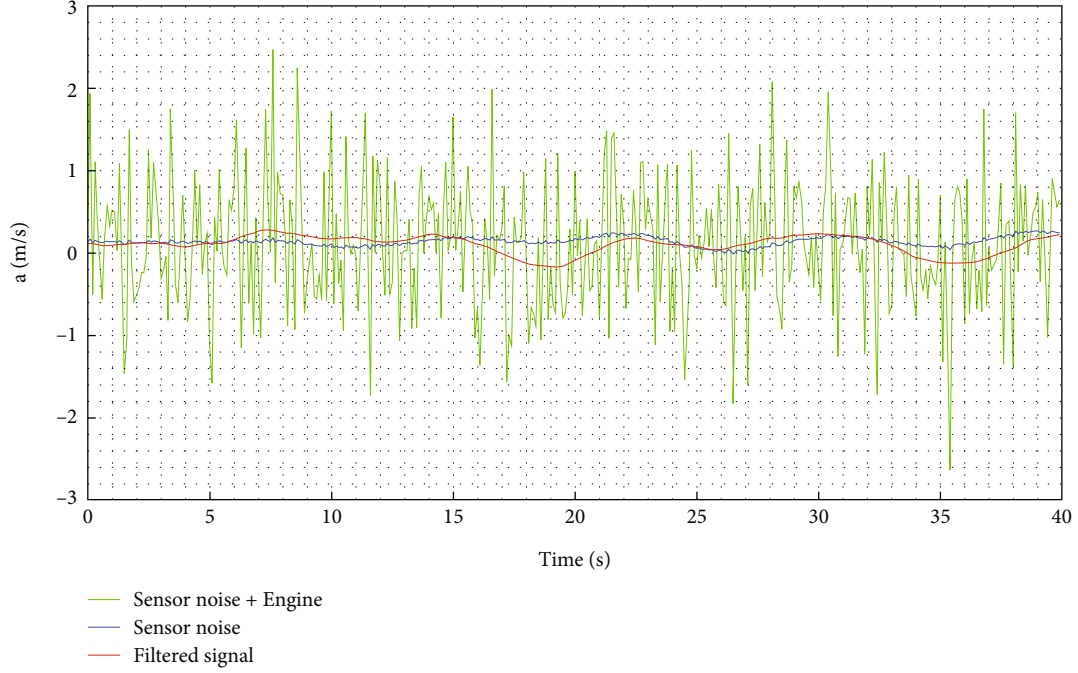
FIGURE 10: Accelerometer error model simulation process for the X-axis and engine.

TABLE 7: Statistical data of original and filtered flight data accelerometer IMU Pixhawk PX4.

Axis	Data	Mean	Standard deviation	Median	Dispersion
X	Unfiltered	1.5391	0.8897	1.7624	0.7917
	Filtered	1.5391	0.8206	1.7627	0.6734
Y	Unfiltered	-0.4376	0.8159	-0.4939	0.6658
	Filtered	-0.4376	0.4668	-0.4981	0.2179
Z	Unfiltered	-10.1512	2.0575	-9.8886	4.2332
	Filtered	-10.1508	1.7718	-9.8889	3.1392

(DCM). The UAV flight speed was 90 km/h, and the flight altitude was set at 50 meters. The input DCM was calculated based on the zero angles of the attack and sideslip angle. The simulation provides the necessary turbulence model, which is suitable for implementation in the filter, where it simulates the real impact of turbulence on UAV control. The turbulence simulation represents the process noise entering the control, shown in Figure 11. The low altitude area is defined by an altitude of up to 305 meters. In this area, the values of turbulence intensity and turbulence rate were defined as follows. The degree of turbulence is a function of height:

$$2L_w = h,$$
$$L_u = 2L_v = \frac{h}{(0.177 + 0.000823h)^{1.2}}. \tag{32}$$

The following is the turbulence intensity:

$$\sigma_w = 0.1W_{20},$$
$$\sigma_u = \sigma_v = \sigma_w \frac{1}{(0.177 + 0.000823h)^{0.4}}, \tag{33}$$

where W_{20} is the wind speed at 6 m.

For weak turbulences, this value was given at a wind speed of 7.72 ms^{-1}; for medium turbulences, it was 15.43 m s^{-1}, and for strong turbulences, it was 23.15 ms^{-1}.

The Kalman filter method can be used to combine the outputs of UAV sensors, which are loaded with various noise mechanisms and faults. The proposed Kalman filter estimates the states of a system that has indeterminate dynamics, shown in Figure 12.

The proposed optimal Kalman filter estimates the immeasurable output of the UAV pitch angle, shown in
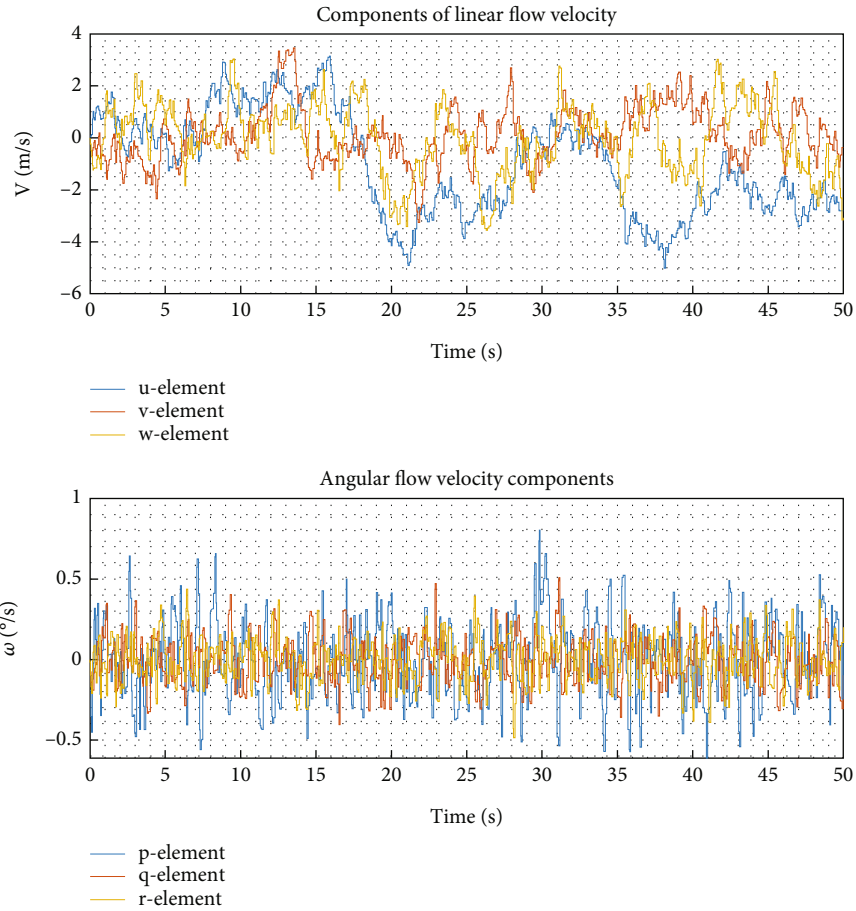
FIGURE 11: Flow components of the UAV from the Dryden wind turbulence model.
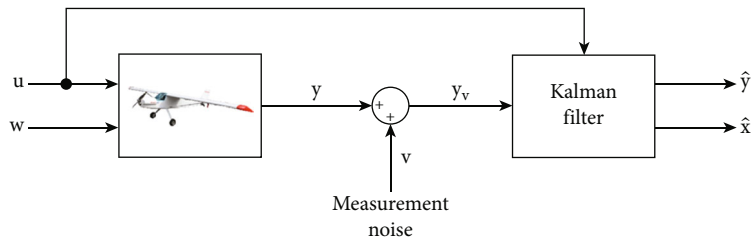

FIGURE 12: Block diagram of the Kalman filter with UAV.

Figure 13. The Kalman filter filters out noisy signals from airspeed, angle of attack, and pitch rate sensors [25]. In the design of the KF, the covariance matrices Q and R proved to be optimal. The diagonal elements of the matrix represent the variations of the individual sensors, and, in the simulations, they had the following values:

$$Q = \begin{bmatrix} 0.01 & 0 & 0 & 0 \\ 0 & 0.01 & 0 & 0 \\ 0 & 0 & 0.001 & 0 \\ 0 & 0 & 0 & 0.001 \end{bmatrix}, \quad (34)$$

$$R = [0.05].$$

The optimization of the Q and R matrices is essential for the best possible KF response to noisy sensor signals, wind gusts, and motor impact. Based on the determined values of the Q and R matrices, the gain was calculated as follows:

$$K_{90} = \begin{bmatrix} -5.6186 * 10^{-7} \\ -0.0056 \\ 0.0216 \\ 0.0110 \end{bmatrix}. \quad (35)$$

Process noise is created by disturbances that affect the UAV during take-off, flight, and landing; these are moments caused by horizontal and vertical airflow. Based on these
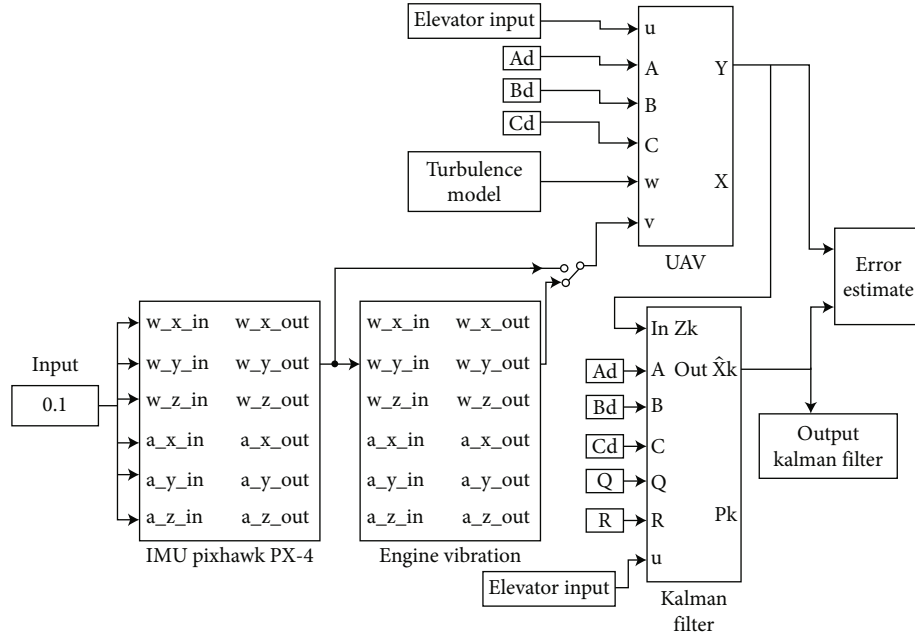
FIGURE 13: Simulation model of the Kalman filter in the longitudinal control of the UAV with the influence of interference.
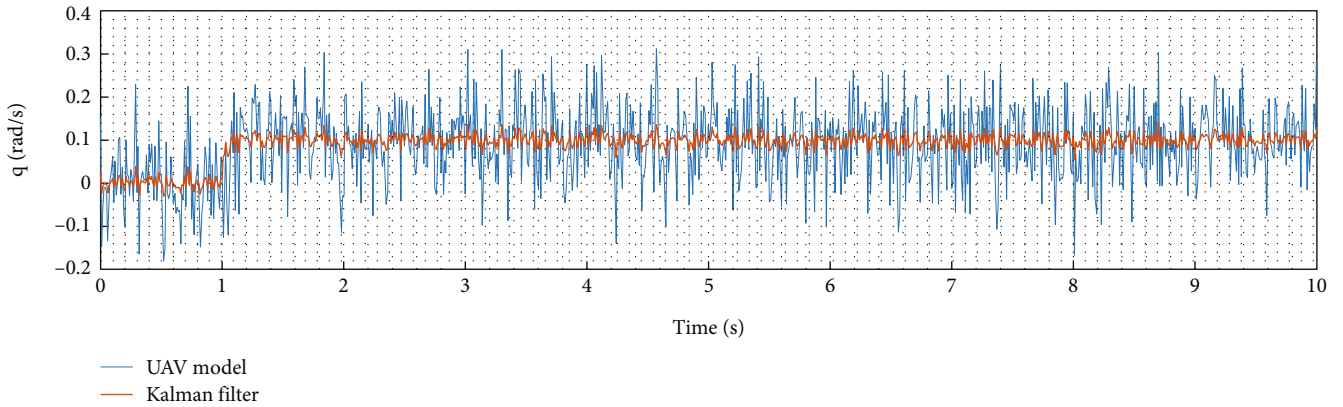

FIGURE 14: Angular velocity output signal from UAV and optimal Kalman filter.

components of the process noise, the error vector of the process v_k (Gaussian white noise with zero mean value) was determined, which has the following form:

$$
w_k = \begin{bmatrix} 0.07 & 0 & 0 & 0 \\ 0 & 0.07 & 0 & 0 \\ 0 & 0 & 0.07 & 0 \\ 0 & 0 & 0 & 0.07 \end{bmatrix}. \tag{36}
$$

The measurement noise was created by the UAV sensors themselves and their error models. Therefore, the definition of the measurement noise was based on the analysis of the Pixhawk PX4 IMU sensors. Based on these measurement noise components, the vector of the measurement errors v_k

(Gaussian white noise with zero mean value) was determined, which has the following form:

$$
v_k = [0.0054]. \tag{37}
$$

The process noise in the assembled model is represented by the q component of the angular flow velocity from the turbulence model. The measurement noise is represented by the noise signal analysed on the Y-axis gyroscope. The output signal of the UAV model was affected by interference signals. The estimate of the Kalman filter has an average error of 0.002°/s as shown in Figure 14, and the estimation of the state of the optimal Kalman filter is shown in Figure 15. The suitability of the selected size of the covariance matrices Q and R is proved by Table 8, which shows the difference in the size of the covariance error at different set values of the covariance matrices Q and R with real input noise.
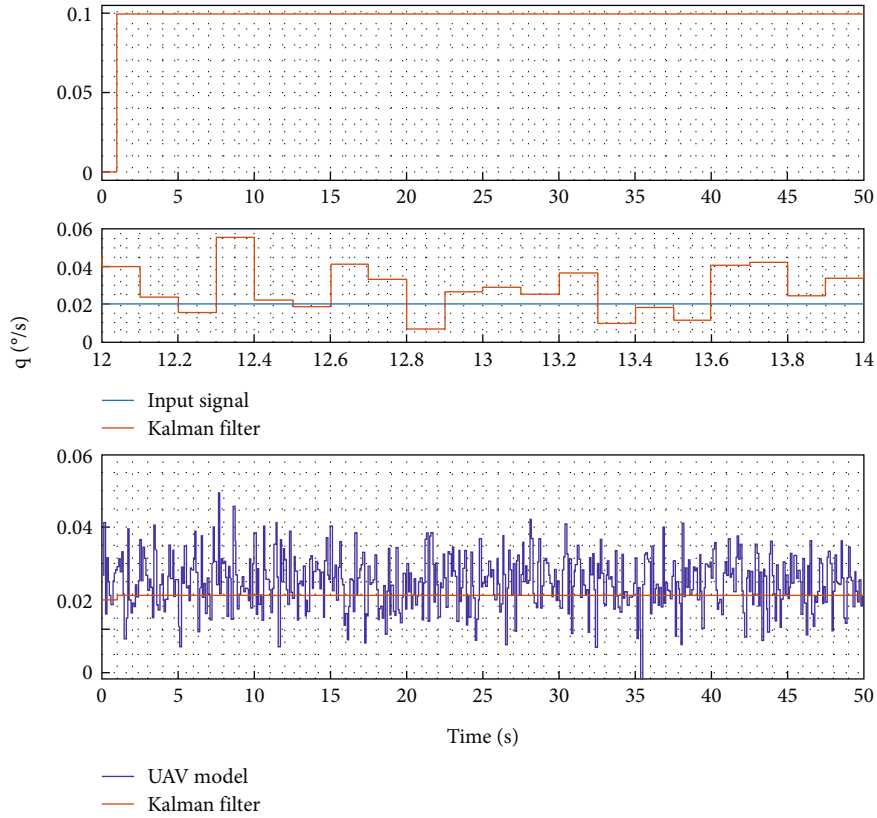
FIGURE 15: Estimation of the state of the optimal Kalman filter.

TABLE 8: Combination covariance errors of the Kalman filter with real input noise.

Matrix values	Before using KF	After using KF
$Q = 0.0001, R = 0.5$		0.01399459
$Q = 0.001, R = 0.5$		0.01401158
$Q = 0.01, R = 0.5$	0.73672095	0.01966605
$Q = 0.0001, R = 0.05$		0.01401158
$Q = 0.0001, R = 0.005$		0.01966595

4. Conclusions

The proposed optimal Kalman filter obtained from the UAV control process eliminates the influence of interfering signals with the required controllability and stability. Because the signals outputted from the IMU sensors serve as feedback to the UAV control system, they must provide real information about position angles and angular velocities. If this information contains noise components, UAV controllability is reduced or lost. Due to this requirement, it was necessary to perform an analysis of IMU Pixhawk PX4 inertial sensors. Error models of the IMU sensors were created, and the sensor measurement outputs were compared with the real static sensor measurement outputs. The values of the biases of the IMU accelerometers and gyroscopes were used for comparison. The results of Allan's sensor analysis are shown in Figure 5. The Y-axis gyroscope was given priority in the analysis of the longitudinal movement of the UAV. The accuracy of the sensor was determined by the standard deviation of the wideband noise and angular random walk (ARW) given in Table 2.

Based on the acquired knowledge, an error model of inertial sensors, a turbulence model, and a model of the longitudinal motion of the "Skydog" aircraft in a discrete state space were created. An optimal Kalman filter model was created, which estimates the state of the angular velocity of the UAV's pitch angle. The results showed that the UAV's longitudinal motion model was significantly disturbed after the connection of measurement noise and process noise, which made UAV control difficult. By connecting the optimal Kalman filter to the UAV control process, the influence of covariance errors on the control process was reduced, as shown in Table 8. The setting of the Kalman filter in the UAV control process was optimal, with an estimated average error of 0.002°/s. The requirements for the created UAV control system were determined by the criteria contained in the identification of the control object so that the control system was robust enough to ensure the stability of the system during various phases of the flight and state of the UAV.

The proposed system improved the phase stability of the UAV. During the entire speed range from 50 km/h to 150 km/h, it had a value of around 68 degrees, and the cutoff frequency varied at -3 dB in the range from 87 rad/s to 219 rad/s.

Data Availability

The numerical data used to support the findings of this study are available from the corresponding author upon request.

Conflicts of Interest

The authors declare that there is no conflict of interest regarding the publication of this manuscript.

Acknowledgments

References

[1] J. T. Jang, A. Santamaria-Navarro, B. T. Lopez, and A. Agha-Mohammadi, "Analysis of state estimation drift on a MAV using PX4 autopilot and MEMS IMU during dead-reckoning," in *2020 IEEE Aerospace Conference*, pp. 1–11, Big Sky, MT, USA, March 2020.

[2] X. Zhang, P. Mumford, and C. Rizos, *Allan Variance Analysis on Error Characters of MEMS Inertial Sensors for an FPGA-Based GPS/INS System*, International Symposium on GPS/GNSS, 2008.

[3] M. Mousa, K. Sharma, and C. G. Claudel, "Inertial measurement units-based probe vehicles: automatic calibration, trajectory estimation, and context detection," *IEEE Transactions on Intelligent Transportation Systems*, vol. 19, no. 10, pp. 3133–3143, 2018.

[4] F. Sadi and R. Klukas, "New jump trajectory determination method using low-cost MEMS sensor fusion and augmented observations for GPS/INS integration," *GPS Solutions*, vol. 17, no. 2, pp. 139–152, 2013.

[5] N. El-Sheimy, H. Hou, and X. Niu, "Analysis and modelling of inertial sensors using Allan variance," *IEEE Transactions on Instrumentation and Measurement*, vol. 57, no. 1, pp. 140–149, 2008.

[6] M. Šipoš, P. Pačes, J. Roháč, and P. Nováček, "Analyses of triaxial accelerometer calibration algorithms," *IEEE sensor Journal*, vol. 12, no. 52, pp. 1157–1165, 2012.

[7] "Dronecode: Windows Cygwin toolchain," 2020, https://dev.px4.io/v1.8.0/en/setup/dev_env_windows_cygwin.html#windows-cygwin-toolchain.

[8] M. A. Al-Mashhadani, "Optimal control and state estimation for unmanned aerial vehicle under random vibration and uncertainty," *Measurement and Control*, vol. 52, no. 9-10, pp. 1264–1271, 2019.

[9] L. Chrif and Z. M. Kadda, "Aircraft control system using LQG and LQR controller with optimal estimation- Kalman filter design," *Procedia Engineering*, vol. 80, pp. 245–257, 2014.

[10] K. T. Borup, T. I. Fossen, and T. A. Johansen, "A nonlinear model-based wind velocity observer for unmanned aerial vehicles," *IFAC-PapersOnLine*, vol. 49, no. 18, pp. 276–283, 2016.

[11] J. W. Langelaan, N. Alley, and J. Neidhoefer, "Wind field estimation for small unmanned aerial vehicles," *Journal of Guidance, Control, and Dynamics*, vol. 34, no. 4, pp. 1016–1030, 2011.

[12] J. T. Li and J. C. Fang, "Sliding average Allan variance for inertial sensor stochastic error analysis," *IEEE Transactions on Instrumentation and Measurement*, vol. 62, no. 12, pp. 3291–3300, 2013.

[13] M. G. Ravi Kumar and T. V. Dr Ramamurthy, "Fault detection of aircraft plant using Kalman filter," *IJCTA*, vol. 8, no. 3, pp. 923–932, 2015.

[14] Y. Zhi, G. Li, Q. Song, K. Yu, and J. Zhang, "Flight control law of unmanned aerial vehicles based on robust servo linear quadratic regulator and Kalman filtering," *International Journal of Advanced Robotic Systems*, vol. 14, no. 1, p. 172988141668695, 2017.

[15] J. Roháč, "Accelerometers and an aircraft attitude evaluation," in *SENSORS, 2005 IEEE*, pp. 784–788, Irvine, CA, USA, October 2005 - November 2005.

[16] J. Roskam, *Flight Dynamics of Rigid and Elastic Airplanes*, University of Kansas Press, Lawrence KS, 1972, Ananth Krishnan & Sinha 22.

[17] M. K. Joyo, D. Hazry, S. F. Ahmed, M. H. Tanveer, F. A. Warsi, and A. Hussain, "Altitude, and horizontal motion control of quadrotor UAV in the presence of air turbulence," in *2013 IEEE Conference on Systems, Process & Control (ICSPC)*, pp. 16–20, Kuala Lumpur, Malaysia, December 2013.

[18] Y. Li, C. Chen, and W. Chen, "Research on longitudinal control algorithm for flying wing UAV based on LQR technology," *International Journal on Smart Sensing and Intelligent Systems*, vol. 6, no. 5, pp. 2155–2181, 2013.

[19] D. L. Halls and J. Llinas, *Handbook of Multisensor Data Fusion*, CRC Press, New York, 2008.

[20] S. J. Julier, J. K. Uhlmann, and H. F. Durrant-Whyte, "A new method for the nonlinear transformation of means and covariances in filters and estimators," *IEEE Transactions on Aerospace and Electronics Systems*, vol. 45, no. 3, pp. 477–482, 2000.

[21] M. S. Arulampalam, S. Maskell, N. Gordon, and T. Clapp, "A tutorial on particle filters for online nonlinear/non-Gaussian Bayesian tracking," *IEEE Transactions on Aerospace and Electronic Systems*, vol. 50, no. 2, pp. 174–188, 2002.

[22] C. Hajiyev, H. E. Soken, and S. Y. Vural, *State Estimation and Control for Low-Cost Unmanned Aerial Vehicles*, Springer, Switzerland, 2015.

[23] R. F. Stengel, *Flight Dynamics*, Princeton University Press, 2004.

[24] N. Lwin and H. M. Tun, "Implementation of flight control system based on Kalman and PID controller for UAV," *International Journal of Scientific and Technology Research*, vol. 3, no. 4, 2014.

[25] A. Ingabire and A. A. Sklyarov, "Control of longitudinal flight dynamics of a fixedwing UAV using LQR, LQG and nonlinear control," *E3S Web of Conferences*, vol. 104, article 02001, 2019.

[26] *IEEE Standard Specification Format Guide and Test Procedure for Single-Axis Interferometric Fiber Optic Gyros*, IEEE Std 952-1997, 1998.

[27] C. Hajiyev and S. Y. Vural, "LQR controller with Kalman estimator applied to UAV," *Chingiz Longitudinal Dynamics*, vol. 4, no. 1, article 28381, p. 6, 2013.

[28] M. Grewal and A. Andrews, *Kalman Filtering Theory and Practice Using MATLAB*, John Wiley & Sons, Inc., New York, NY USA, 2 edition, 2001.

[29] D. Megyesi, R. Bréda, and M. Schrötter, "Adaptive control and estimation of the condition of a small unmanned aircraft using a Kalman filter," *Energies*, vol. 14, no. 8, p. 2292, 2021.

[30] A. M. Kamal, A. A. Bayoumy, and A. Elshabka, "Modeling, analysis and validation of a small airplane flight dynamics," in *AIAA Modeling and Simulation Technologies Conference*, Kissimmee, Florida, January 2015.

[31] J. Llobera Capllonch, *Longitudinal Stability Control System Design for the UAV Ultra Stick 25e*, Universitas Politècnica de Catalunya, 2015.